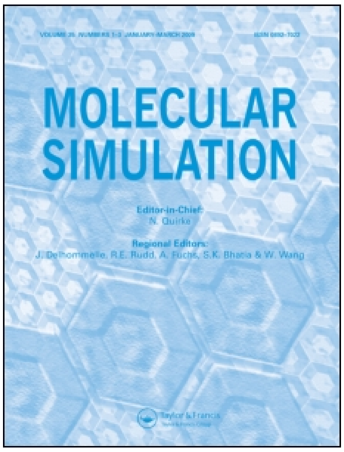

Molecular Simulation
Publication details, including instructions for authors and subscription information:
http://www.informaworld.com/smpp/title~content=t713644482

A DFT computational study of phosphine ligand dissociation *versus* hemilability in a Grubbs-type precatalyst containing a bidentate ligand during alkene metathesis

M. Jordaan[a]; H. C. M. Vosloo[a]
[a] School of Chemistry, North-West University, Potchefstroom, South Africa

To cite this Article Jordaan, M. and Vosloo, H. C. M.(2008) 'A DFT computational study of phosphine ligand dissociation *versus* hemilability in a Grubbs-type precatalyst containing a bidentate ligand during alkene metathesis', Molecular Simulation, 34: 10, 997 — 1012

To link to this Article: DOI: 10.1080/08927020802411737

URL: http://dx.doi.org/10.1080/08927020802411737

Molecular Simulation
Vol. 34, Nos. 10–15, September–December 2008, 997–1012

A DFT computational study of phosphine ligand dissociation *versus* hemilability in a Grubbs-type precatalyst containing a bidentate ligand during alkene metathesis

M. Jordaan and H.C.M. Vosloo*

School of Chemistry, North-West University, Potchefstroom, South Africa

(*Received 7 February 2008; final version received 12 August 2008*)

Using density functional theory, the metathesis reaction of 1-octene in the presence of a Grubbs-type ruthenium alkylidene complex bearing a chelating pyridinyl alcoholate ligand, [RuCl(L)(O^N)(=CHPh)] (L = H_2IMes or PCy_3, O^N = 1-(2′-pyridinyl)cyclohexan-1-olate)), was investigated. The complete geometry optimisation and activation energy of various activation steps in the dissociative mechanism were performed at the GGA-PW91/DNP level of theory using Accelrys Materials Studio® 4.0. Two possible precatalyst initiations were explored, i.e. the dissociation of the labile N-atom of the O^N-ligand as well as the dissociation of ligand L, due to the belief that ruthenium-catalysed metathesis reactions proceed through 14-electron intermediates. The formation of the catalytically active heptylidene species is kinetically favoured for both the first- and second-generation chelating complexes. The computational results are in agreement with the experimental results obtained with NMR for the second-generation system. The computational results suggest that both phosphine ligand dissociation and hemilability may play a role in the metathesis reaction with the first-generation system.

Keywords: DFT; alkene metathesis; Grubbs-type precatalyst; hemilabile ligand

1. Introduction

Research in coordination and organometallic chemistry, strongly supported in the last decade by theoretical studies [1–13], has provided much insight into the mechanism of catalytic processes involving M—C or M—H bonds. Alkene metathesis is one such example of a catalytic process involving M—C bonds that has been successfully applied in both academic and industrial environments with combined experimental and theoretical support [8,10,14]. This resulted in the calculation of certain mechanistic parameters for the alkene metathesis mechanism with ruthenium carbenes [6,7,9,10,12,15–20]. However, these studies focused on the catalytic cycle and ligand dissociation of the methylidene species $RuCl_2(PR_3)_2(=CH_2)$ with model PR_3 (R = H, Me) ligands and/or ethene as model substrate to mainly reduce the computing cost. Therefore, the steric and electronic influence of the actual ligands (PCy_3 *versus* PR_3, (R = H, Me)) and substrates (1-octene *versus* ethene) with the benzylidene complex (*versus* methylidene complex) as precatalyst were not taken into consideration. Nonetheless, with the use of molecular modelling a deeper insight was gained into the mechanism of the alkene metathesis reaction.

The increasing interest in more stable and catalytically active systems for metathesis reactions has encouraged various researchers to modify the well-defined, highly active and robust ruthenium-based Grubbs systems, $RuCl_2(PCy_3)L(=CHPh)$ [L = PCy_3 (**I**) or H_2IMes (**II**)] with the incorporation of chelating ligands (note: H_2IMes is a N-heterocyclic carbene ligand commonly abbreviated as NHC). Hemilabile ligands, a class of chelating ligands, have the ability to increase the thermal stability of the ruthenium carbene complexes by releasing a coordination site 'on demand' of *inter alia* an alkene (such as norbornene) and occupying it otherwise – thus preventing decomposition via free coordination sites (Scheme 1) [21–25].

In a previous study [25], we investigated the 1-octene metathesis reaction with a hemilabile first- (**III**) and second-generation (**IV**) Grubbs-type precatalyst with the use of ^{1}H NMR. The results suggested that two different mechanisms might be involved for **III** and **IV**, since five carbene species were observed during the 1-octene metathesis reaction with **IV**, while only three carbene species were visible in the presence of **III** [25]. However, it was observed that in the presence of **IV** at 50°C in $CDCl_3$ the heptylidene is the catalytically active species that preferentially forms during the 1-octene metathesis reaction, while both the heptylidene and methylidene species form simultaneously during the reaction with **III**. This necessitated a computational investigation of the alkene metathesis reaction with a hemilabile precatalyst

---

*Corresponding author. Email: manie.vosloo@nwu.ac.za

ISSN 0892-7022 print/ISSN 1029-0435 online

DOI: 10.1080/08927020802411737
http://www.informaworld.com

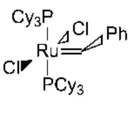

I

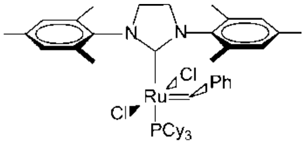

II

Structures **I** and **II**

to gain more insight into the mechanism of this reaction. Therefore, in this study we investigated the dissociative 1-octene metathesis mechanism with **III** and **IV** according to a conceptual model we proposed for the productive dissociative mechanism of the 1-octene metathesis reaction in the presence of **I** [8]. The computational results from this model were in agreement with the experimental results obtained with NMR and GC/MSD (Mass Selective Detector) experiments, in which it was indicated that the heptylidene species was the catalytically active species that preferentially formed in the 1-octene metathesis reaction with **I** [8].

2. Experimental

2.1 Computational details

The quantum chemical calculations were carried out by density functional theory (DFT) since it usually gives realistic geometries, relative energies and vibrational frequencies for transition metal compounds. All calculations were performed with the DMol^3 DFT code [26] as implemented in Accelrys Materials Studio® 4.0 (http://www.accelrys.com/) on either a 4 CPU (HP Proliant CP4000) or a 52 CPU cluster (HP Proliant CP4000 Linux Beowulf with Procurve Gb/E Interconnect on compute nodes) (http://www.hp.com). The non-local generalised gradient approximation (GGA) functional by Perdew and Wang (PW91)[27] was used for all geometry optimisations. The convergence criteria for these optimisations consisted of threshold values of 2×10^{-5} Ha, 0.004 Ha/Å and 0.005 Å for energy, gradient and displacement convergence, respectively, while a self-consistent field density convergence threshold value of 1×10^{-5} Ha was specified. DMol^3 utilises a basis set of numeric atomic functions, which are exact solutions to the Kohn–Sham equations for the atom [28]. These basis sets are generally more complete than a comparable set of linearly independent Gaussian functions and have been demonstrated to have small basis set superposition errors [28]. In this study, a polarised split valence basis set, termed double numeric polarised (DNP) basis set was used. All geometry optimisations employed highly efficient delocalised internal coordinates [29]. The use of delocalised coordinates significantly reduces the number of geometry optimisation iterations needed to optimise larger molecules compared with the use of traditional Cartesian coordinates. Some of the geometries optimised were also subjected to full frequency analyses at the same GGA/PW91/DNP level of theory to verify the nature of the stationary points. Equilibrium geometries were characterised by the absence of imaginary frequencies. Preliminary transition state (TS) geometries were obtained by the integrated linear synchronous transit/quadratic synchronous transit algorithm available in Materials Studio 4.0. This approach was used before in computational studies in homogeneous alkene trimerisation and metathesis [11,30]. These preliminary structures were then subjected to full TS optimisations using an eigenvector following algorithm. For selected TS geometries, confirmation calculations involving intrinsic reaction path (IRP) calculations were performed in which the path connecting reagents, TS and products were mapped. The IRP technique used in Materials Studio 4.0 also corresponds to the intuitive minimum energy pathway connecting two structures and is based on the nudged elastic band algorithm of Henkelman and Jonsson [31]. The IRP calculations, performed at the same GGA/PW91/DNP level of theory, ensured the direct connection of TSs with the respective reactant and product geometries. All transition structure geometries exhibited only one imaginary frequency in the reaction coordinate. All results were mass balanced for the isolated system in the gas phase. The energy values that are given in the results are the electronic energies at 0 K and therefore only the electronic effects are in consideration in this paper. For the purpose of this study the minimum structure obtained from the geometry optimisation (GGA/PW91/DNP) of 1-octene was used in further calculations. In this structure, the hexyl-chain was 'straight' and remained so in most of the optimisations of intermediates. The influence of the various confirmations of 1-octene on the energetics of the reaction pathway was not considered in this study.

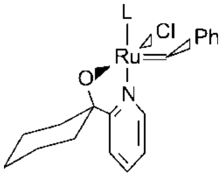

L = PCy$_3$ (**III**)
= H$_2$IMes (**IV**)

Structures **III** and **IV**

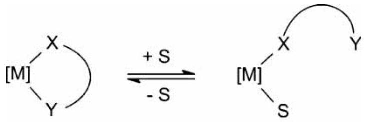

S = substrate
X = tightly bound group
Y = labile group

Scheme 1. Schematic representation of the concept of hemilability [21–25].

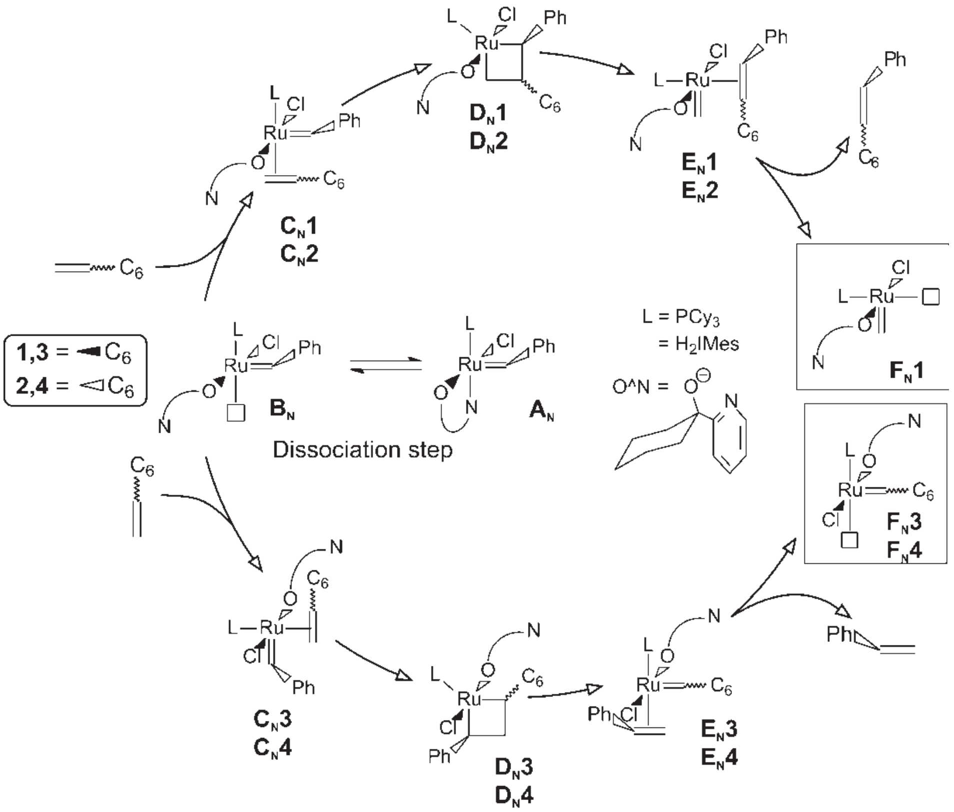

Scheme 2. Dissociation ($\mathbf{A_N}$ to $\mathbf{B_N}$) and activation ($\mathbf{B_N}$ to $\mathbf{F_N}$) steps in the mechanism of productive 1-octene metathesis using $RuCl_2(PCy_3)L(O^\wedge N)(=CHPh)$ ($L = PCy_3$ or H_2IMes, $O^\wedge N$ = 1-(2′-pyridinyl)cyclohexan-1-olate).

2.2 *Model system and notation*

Conceptually, the productive metathesis of 1-octene in the presence of the hemilabile Grubbs carbene complexes are illustrated in Schemes 2 and 3. The mechanism is initiated by either dissociation of the labile N-atom of the O,N-chelating ligand (Scheme 2), or the dissociation of the phosphine or NHC ligand from the respective first- and second-generation hemilabile carbenes (Scheme 3).

The generic labels **A**–**F** are given to the individual hemilabile ruthenium carbene and derived species involved in the conceptualised reaction mechanism. The mechanism consists of either the dissociation of the labile N-atom of the O,N-chelating ligand from **III** or **IV** ($\mathbf{A_N}$) to yield RuCl(L)(O^N-open)(=CHPh) [$L = PCy_3$ (**III**) or H_2IMes (**IV**)] ($\mathbf{B_N}$) or the loss of L ($L = PCy_3$ or H_2IMes) to yield RuCl(O^N)(=CHPh) ($\mathbf{B_L}$). The different stereochemical approaches of 1-octene towards the catalytically active species **B** leads to four activation steps (**1**–**4** notations). To identify which step is under consideration, a numerical suffix (**1**–**4**) is associated with the labels **C**—**F** (e.g. $\mathbf{C_N1}$ to $\mathbf{F_N1}$ represents activation step 1 when the labile N-atom of the O,N-chelating ligand is dissociated) and the additional subscript **N** or **L** indicates the dissociated ligand under consideration, i.e. **N** for the dissociation of the labile N-atom of the O,N-chelating ligand and **L** for the dissociation of the ligand L ($L = PCy_3$ for **III** and L = NHC for **IV**). TSs are denoted analogously, e.g. $\mathbf{C_L3}$–$\mathbf{D_L3}$ is the TS for the conversion of $\mathbf{C_L3}$ to $\mathbf{D_L3}$ when L is dissociated from $\mathbf{A_L}$.

3. Results and discussion

3.1 *Catalyst initiation*

It is generally accepted that the Ru-catalysed alkene metathesis reaction proceeds via a dissociative mechanism, which is initiated by the dissociation of a phosphine ligand from $RuX_2(PR_3)L(=CHR)$ to form a 14-electron species (‘**B**’) [6,15,32]. In this sense, catalyst initiation involves the dissociation of PCy_3 for both **I** and **II**. However, catalyst initiation of hemilabile complexes is more complex since both a dissociative or associative mechanism may play a role during the initiation and activation phases. This is due to the belief that a hemilabile ligand releases a free coordination site ‘on demand’ of competing substrates and occupy it otherwise [24]. As illustrated in Scheme 4, the ruthenium centre of the hemilabile complexes might become coordinatively unsaturated with or without the influence of the incoming alkene.

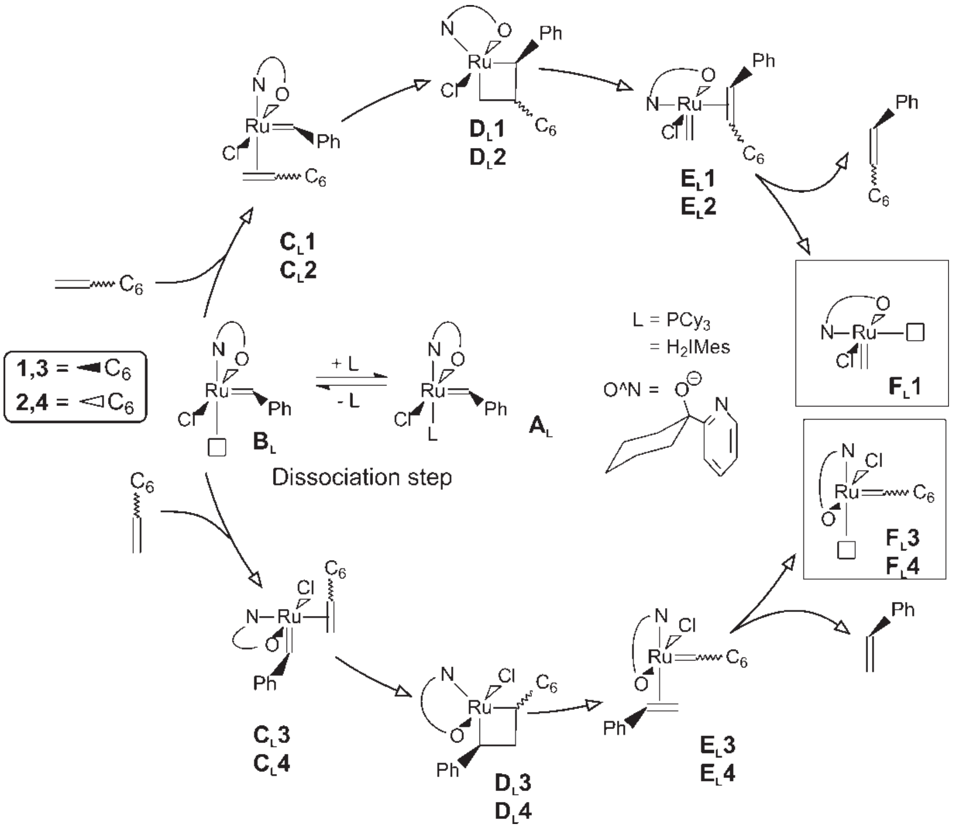

Scheme 3. Dissociation ($\mathbf{A_L}$ to $\mathbf{B_L}$) and activation ($\mathbf{B_L}$ to $\mathbf{F_L}$) steps in the mechanism of productive 1-octene metathesis using $RuCl_2(L)(O^\wedge N)(=CHPh)$ ($L = PCy_3$ or H_2IMes, $O^\wedge N$ = 1-(2′-pyridinyl)cyclohexan-1-olate).

In this study, two possible precatalyst initiations of only the dissociative mechanism was theoretically investigated, i.e. (a) the dissociation of the labile N-atom of the O^N-ligand (Scheme 5(a)) and (b) the dissociation of ligand L (with $L = PCy_3$ or H_2IMes; Scheme 5(b)). This was as a result of free PCy_3 ligand being observed experimentally with GC/FID (Flame Ionization Detector) throughout the 1-octene metathesis investigations in the presence of the first-generation hemilabile complexes [8].

Although various orientations of the alkylidene moiety in ‘**B**’ is possible (Figure 1), this was not explored in detail, since it has been shown that the **B1**-orientation of the alkylidene is lower in energy for the Grubbs first- and second-generation methylidene species [10]. Therefore, complexes corresponding to ‘**B1**’ were used as starting structures prior to optimisations. Spontaneous formation of the perpendicular alkylidene orientation (‘**B2**’) resulted during optimisation of the unsaturated **I**, **III** and **IV** benzylidene complexes, while remaining parallel for the second-generation Grubbs system (**II-B1**). The Ph-ring of the alkylidene rotated upward towards the PCy_3 for the first-generation systems while the steric bulk on NHC caused the Ph-ring to rotate downward into the open coordination site for **IV**.

Table 1 summarises the calculated electronic (ΔE) energies in kcal/mol for the initiation phase (‘**A**’ – ‘**B**’) of the 1-octene metathesis reaction in the presence of **I**–**IV** according to the dissociation of the N-atom or L.

Dissociation of PCy_3 from the Grubbs first-generation 16-electron precatalyst complex (**I-A**) proceeds with $\Delta E = 21.89$ and 25.92 kcal/mol for the second-generation precatalyst (**II-A**). This is in agreement with the experimental kinetic studies by Grubbs [15,32] in which $\Delta H^\ddagger$ values

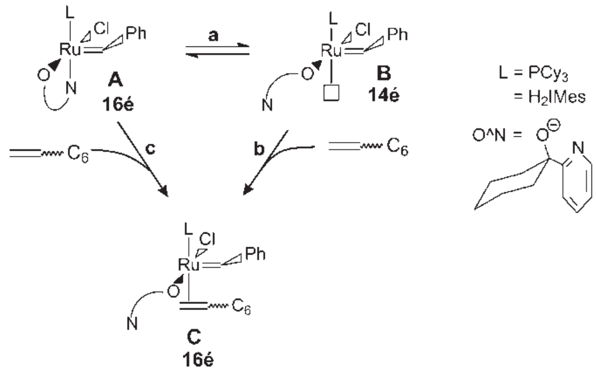

Scheme 4. Illustration of the dissociative (a and b) and associative (c) catalyst initiation steps for **III** and **IV**.

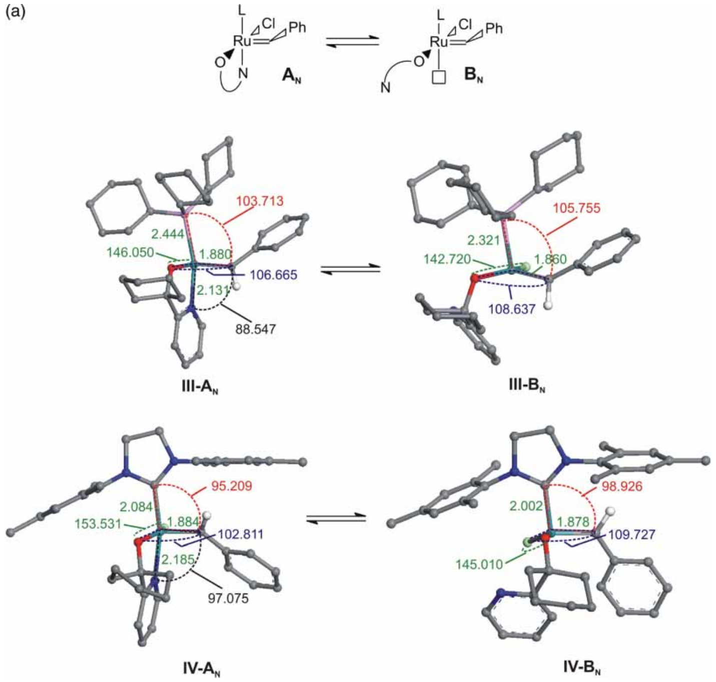

Scheme 5(a). Dissociation ($\mathbf{A_N}$ to $\mathbf{B_N}$) of labile N-atom of O,N-ligand along with the optimised geometries for the lowest energy catalyst precursor complexes. The hydrogen atoms on the ligands are omitted for clarity and the unit of the indicated bond distances is angstrom (Å).

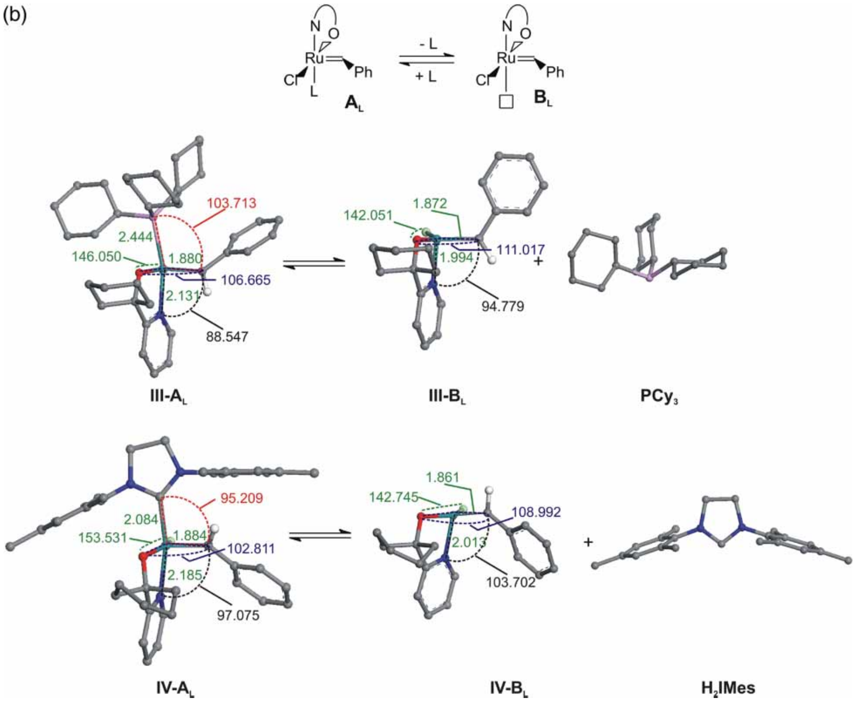

Scheme 5(b). Dissociation ($\mathbf{A_L}$ to $\mathbf{B_L}$) of ligand L along with the optimised geometries for the lowest energy catalyst precursor complexes. The hydrogen atoms on the ligands are omitted for clarity and the unit of the indicated bond distances is angstrom (Å).

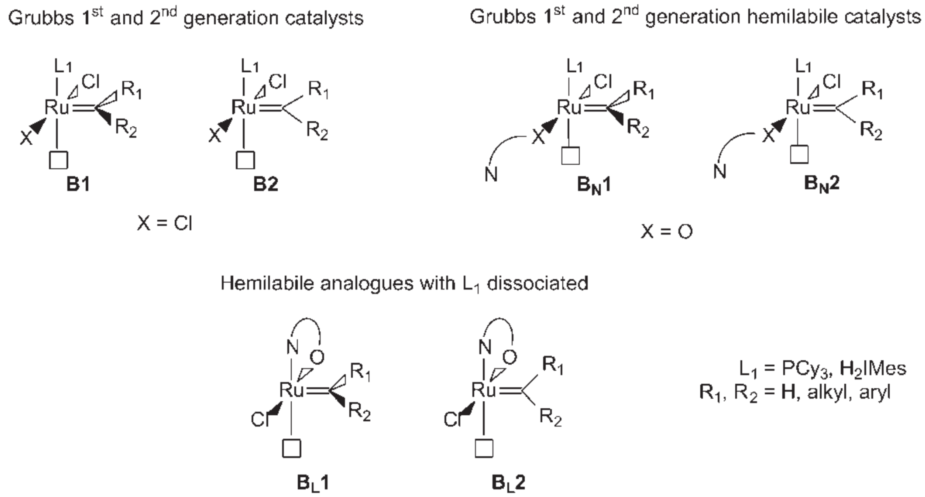

Figure 1. Illustration of the possible orientations of the alkylidene moiety for the Ru–carbene unsaturated complexes.

Table 1. Calculated electronic (ΔE) energies in kcal/mol for the initiation phase sequence '**A**'–'**B**' as catalysed by **I**–**IV**.

Mechanistic sequence #	I	II	III	IV
A	0.0	0.0	0.0	0.0
$\mathbf{B_L}$	21.89[a]	25.92[a]	23.26[a]	61.52[b]
$\mathbf{B_N}$	–	–	20.26	16.08

All energies are reported relative to the respective precatalysts '**A**' and balanced with the energies of free ligand, where necessary.[a] Dissociation of L = PCy_3. [b] Dissociation of L = H_2IMes, no PCy_3 ligands are present in this complex.

of 23.6 ± 0.5 and 27 ± 2 kcal/mol were obtained for **I** and **II**, respectively.

The dissociation of PCy_3 in the first-generation hemilabile analogue **III-A** ($\mathbf{III\text{-}B_L}$ $\Delta E = 23.26$ kcal/mol) is calculated to be 3 kcal/mol less favourable than the dissociation of the labile N-atom of the O^N-bidentate ligand ($\mathbf{III\text{-}B_N}$). This implies that **III** might rather initiate via the dissociation of the labile N-atom, which compared to **I**, is *ca.* 1.5 kcal/mol more favourable. Although $\mathbf{III\text{-}B_L}$ is *ca.* 3 kcal/mol less favourable than $\mathbf{III\text{-}B_N}$, it is only 1.5 kcal/mol less favourable than **I**, and should therefore not be completely discarded. Only after investigating the complete mechanism, i.e. initiation, activation and catalytic cycle, can concluding remarks be made with regards to which dissociation step $\mathbf{B_N}$ or $\mathbf{B_L}$ is favoured. The dissociation of H_2IMes in the second-generation hemilabile analogue **IV-A** ($\mathbf{IV\text{-}B_L}$, $\Delta E = 61.52$ kcal/mol) is found to be more unfavourable (45 kcal/mol) than the dissociation of the labile N-atom ($\mathbf{IV\text{-}B_N}$). This suggests that **IV** also initiates via the dissociation of the labile N-atom ($\Delta E = 16.08$ kcal/mol), which compared to **II**, is *ca.* 10 kcal/mol more favourable. However, the possibility of another mechanistic route dominating *inter alia* an associative coordination of the alkene prior to dissociation of the labile N-atom cannot be excluded entirely.

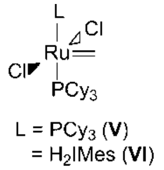

Structures **V** and **VI**

3.2 *Activation phase*

After catalyst initiation, an alkene coordinates to the unsaturated intermediate species '**B**' to form the corresponding π-complexes '**C**'. The alkene can coordinate in two discrete, perpendicular orientations trans to L for the various

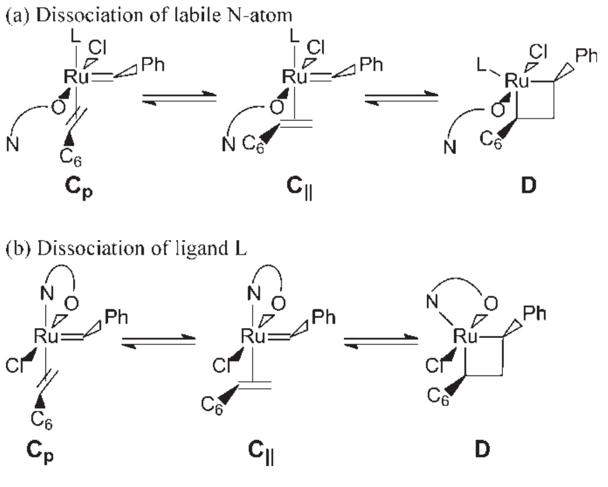

Scheme 6. *Trans*-alkene coordination in the dissociative pathway for the Grubbs hemilabile precatalysts (L = PCy_3 or H_2IMes). (a) Dissociation of labile N-atom and (b) dissociation of ligand L.

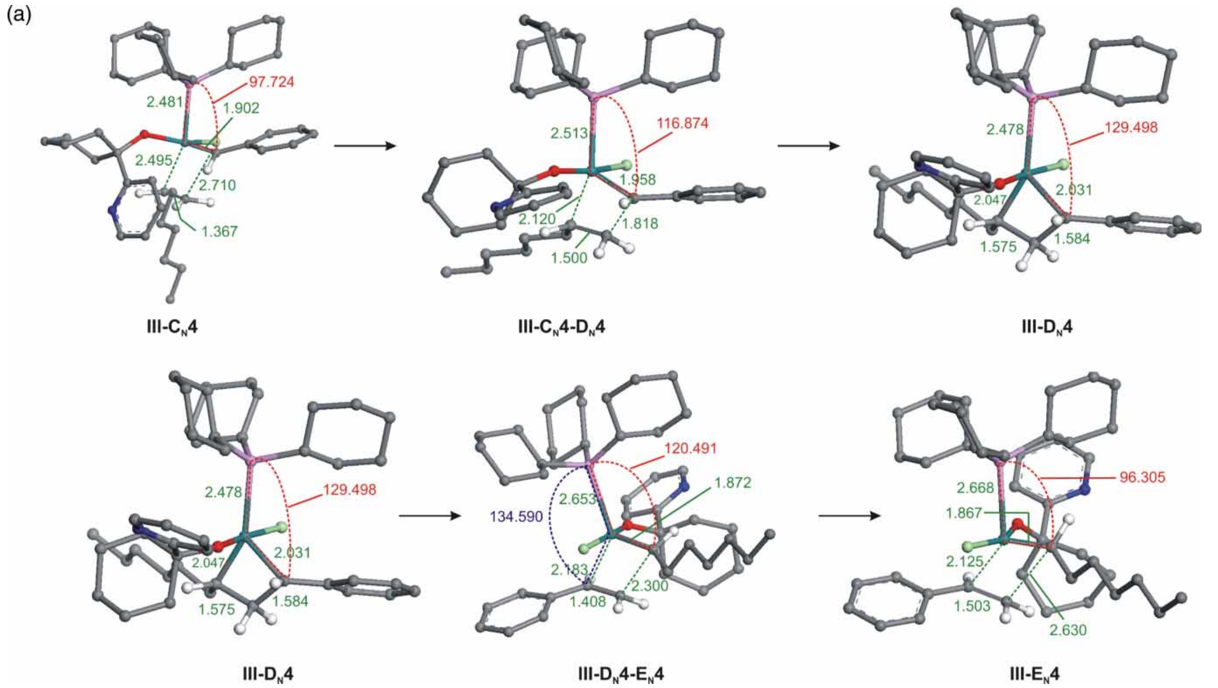

Scheme 7(a). Optimised geometries of the lowest energy equilibrium and TS structures involved in the metathesis reaction with **III** for activation step 4 ($\mathbf{C_N}$ to $\mathbf{E_N}$) in the $\mathbf{C_{II}}$ mode when the labile N-atom is dissociated. The hydrogen atoms on the ligands are omitted for clarity and the unit of the indicated bond distances is angstrom (Å).

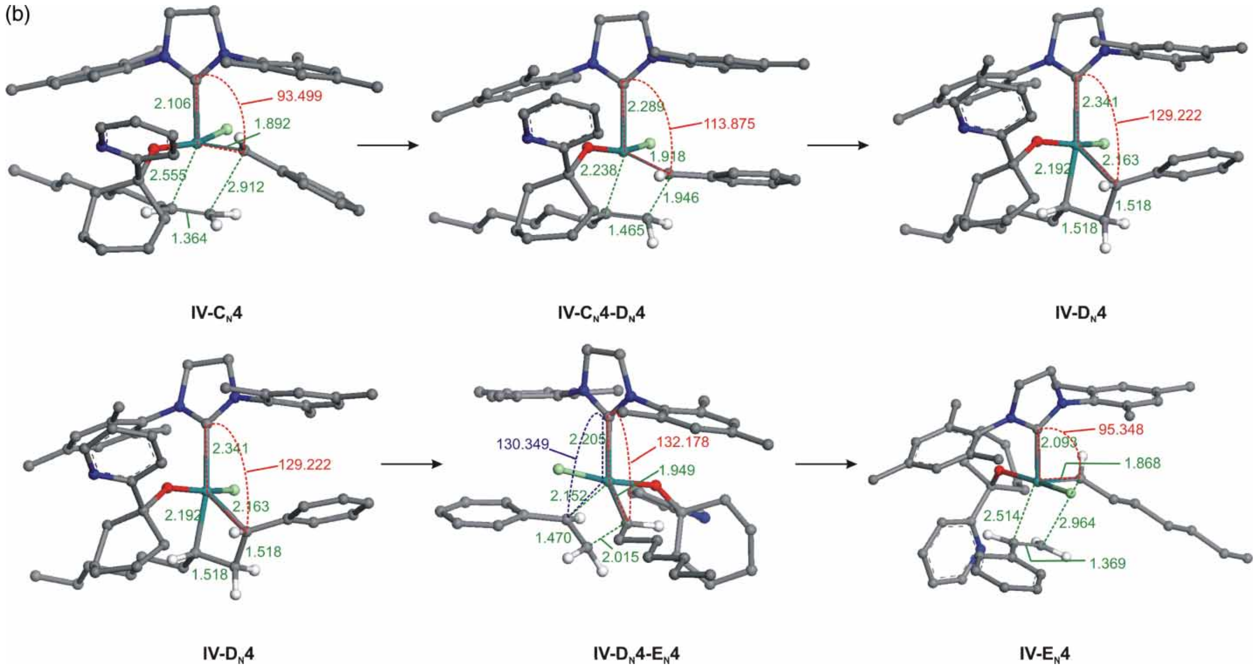

Scheme 7(b). Optimised geometries of the lowest energy equilibrium and TS structures involved in the metathesis reaction with **IV** for activation step 4 ($\mathbf{C_N}$ to $\mathbf{E_N}$) in the $\mathbf{C_{II}}$ mode when the labile N-atom is dissociated. The hydrogen atoms on the ligands are omitted for clarity and the unit of the indicated bond distances is angstrom (Å).

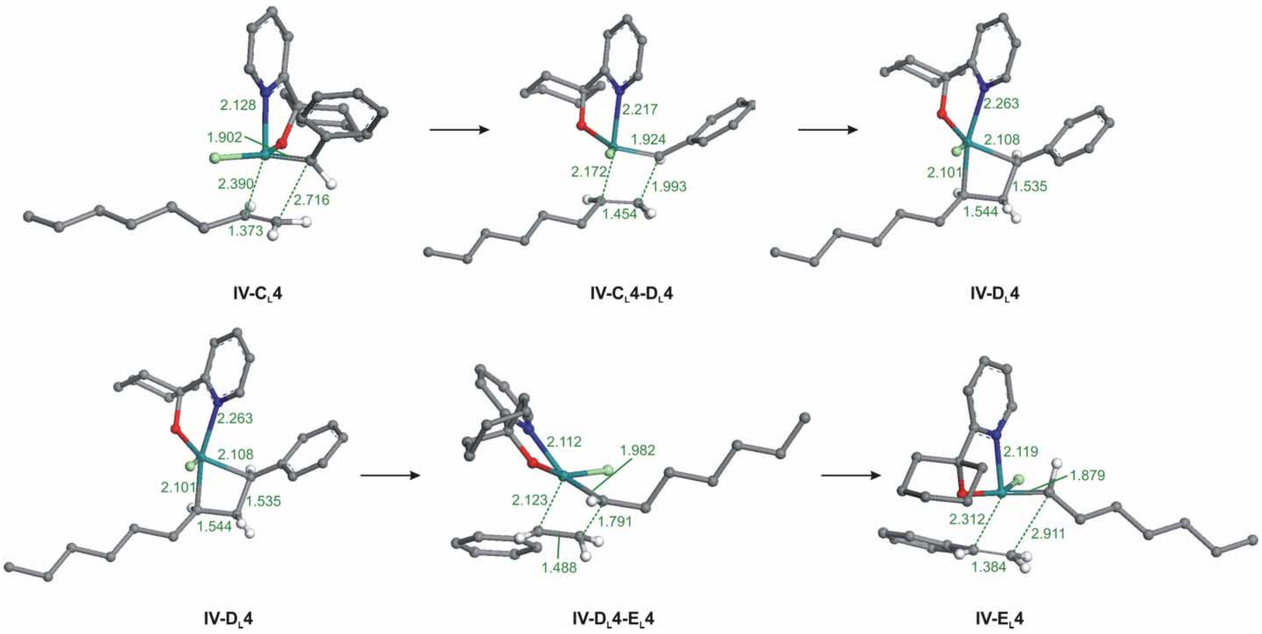

Scheme 8. Optimised geometries of the lowest energy equilibrium and TS structures involved in the metathesis reaction with **IV** for activation step 4 (**C$_L$** to **E$_L$**) in the **C$_{II}$** mode when L is dissociated. The hydrogen atoms on the ligands are omitted for clarity and the unit of the indicated bond distances is angstrom (Å).

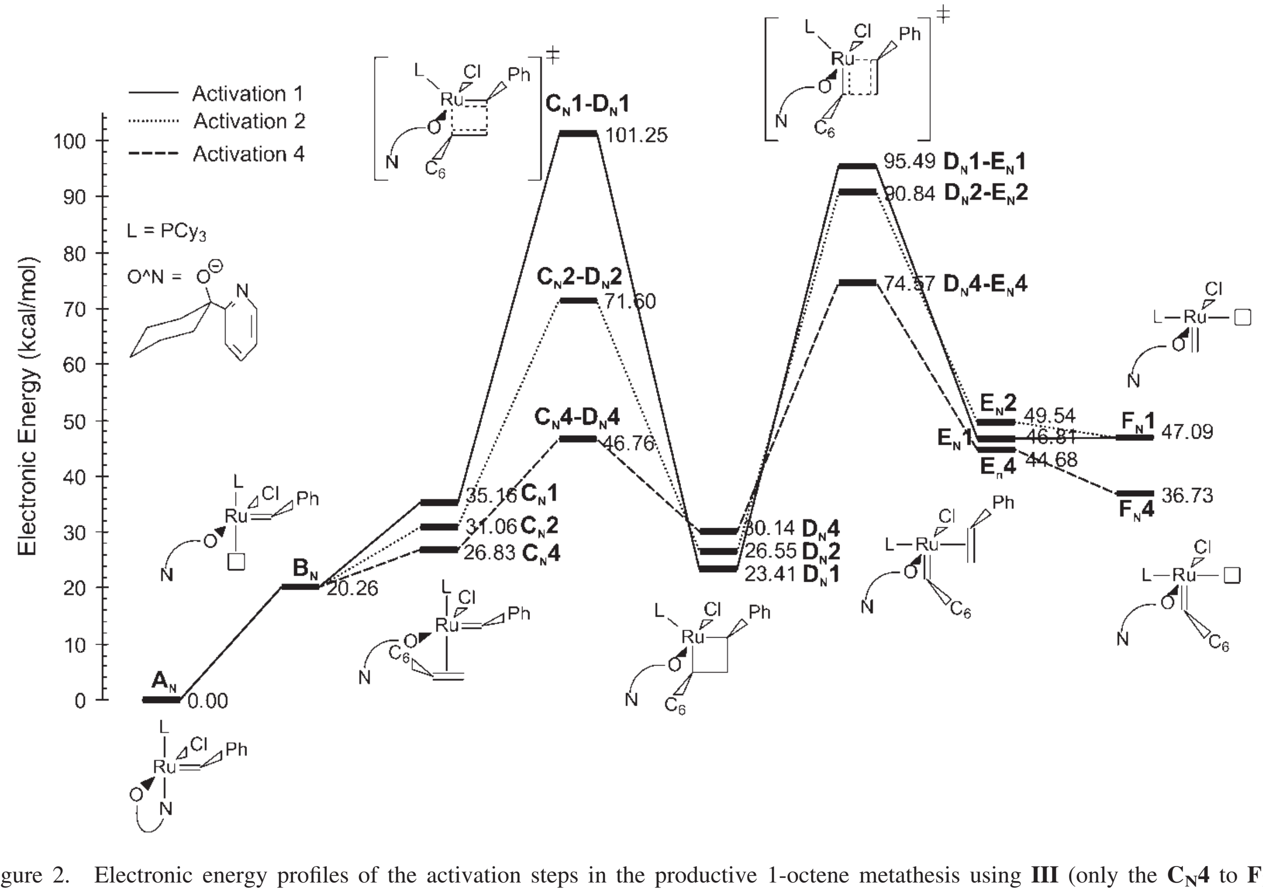

Figure 2. Electronic energy profiles of the activation steps in the productive 1-octene metathesis using **III** (only the **C$_N$4** to **F$_N$4** structures are shown; **C$_p$ mode**).

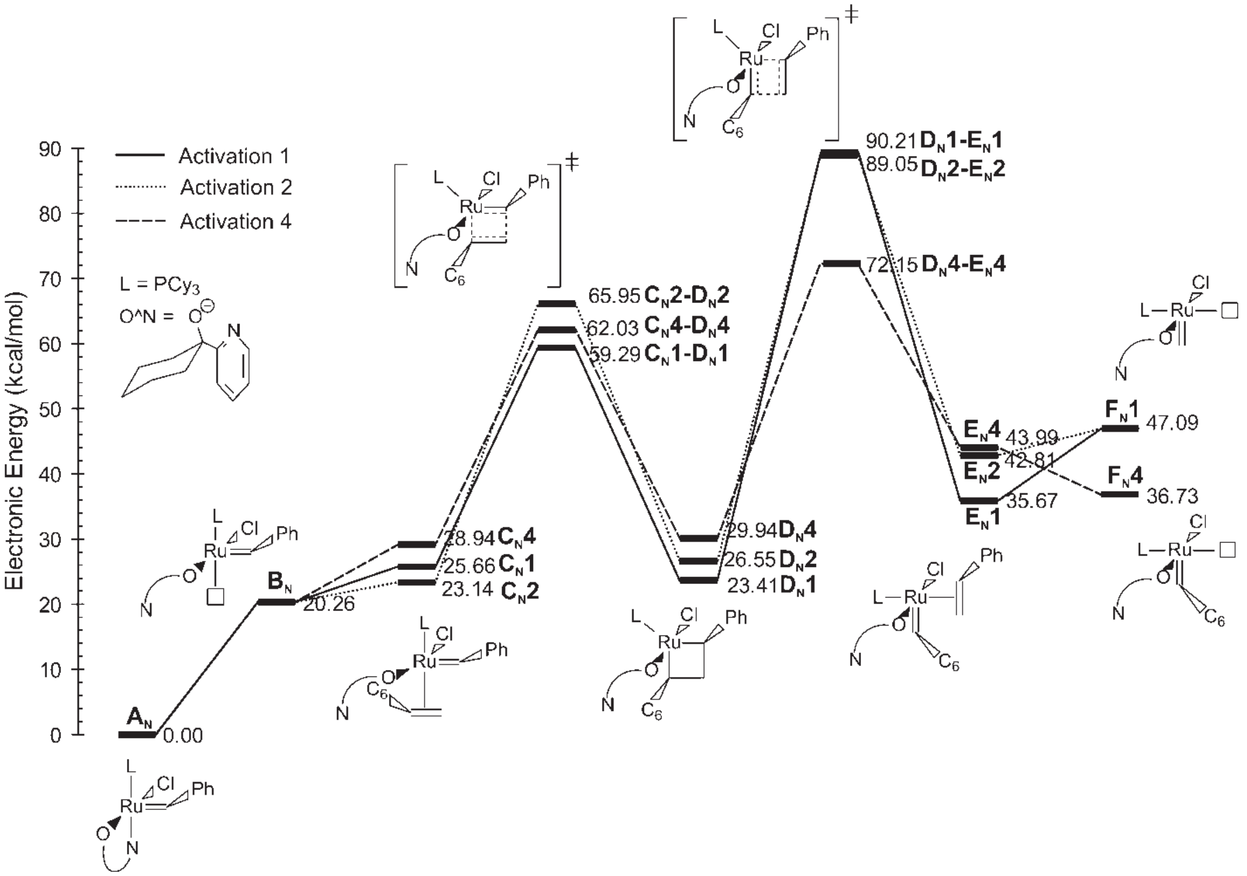

Figure 3. Electronic energy profiles of the activation steps in the productive 1-octene metathesis using **III** (only the $\mathbf{C_N4}$ to $\mathbf{F_N4}$ structures are shown; $\mathbf{C_{II}}$ mode).

Ru═C systems (Scheme 6). In a recent study [10], it was shown that the coordination of the alkene in the $\mathbf{C_{II}}$ mode is energetically more favoured for the first- and second-generation Grubbs methylidene complexes (**V** and **VI**). However, both the $\mathbf{C_p}$–$\mathbf{C_{II}}$–**D** and $\mathbf{C_{II}}$–**D** conversion was investigated for the hemilabile analogues, to determine whether the bidentate ligand will influence the stability of the various intermediates. The optimised geometries of the lowest energy equilibrium and TS structures involved in the metathesis reaction with **III** and **IV** for activation step 4 in the $\mathbf{C_{II}}$ mode are given in Scheme 7 (the labile N-atom is dissociated, L = PCy_3 (Scheme 7(a)) and H_2IMes (Scheme 7(b))) and Scheme 8 (L = PCy_3 or H_2IMes is dissociated). For the sake of simplicity all structures in the electronic profile Figures (Figures 2–8) are drawn in the $\mathbf{C_{II}}$ mode. However, in the text the $\mathbf{C_p}$–$\mathbf{C_{II}}$–**D** conversions will be referred to as the $\mathbf{C_p}$ mode, while the $\mathbf{C_{II}}$ mode will refer to the $\mathbf{C_{II}}$–**D** conversions.

3.2.1 *When the labile N-atom is dissociated from* ***III*** *and* ***IV***

Figures 2 and 4 illustrate the activation steps for the $\mathbf{C_p}$ mode of **III** and **IV**, while Figures 3 and 5 illustrate the steps for the $\mathbf{C_{II}}$ mode according to Scheme 1. The relative energies for the optimised structures are summarised in Table 2. Activation step 3 is not shown for the hemilabile systems because of its similarity to activation step 4. No energy barriers were calculated for the dissociation of the labile N-atom or the association of the alkene since it was assumed that these steps proceed without considerable rearrangement of the complex. This should be investigated further to take the rotation of the hemilabile ligand around the Ru—O-bond into consideration.

Activation step 4 ($\mathbf{B_N}$ to $\mathbf{C_N4}$ to $\mathbf{F_N4}$) is thermodynamically and kinetically more favourable than activation steps 1 ($\mathbf{B_N}$ to $\mathbf{C_N1}$ to $\mathbf{F_N1}$) and 2 ($\mathbf{B_N}$ to $\mathbf{C_N2}$ to $\mathbf{F_N1}$; note $\mathbf{F_N2} = \mathbf{F_N1}$) for both systems in the $\mathbf{C_p}$ and $\mathbf{C_{II}}$ mode (Figures 2–5). However, the modelling results for **IV** cannot explain the observed ^{1}H NMR results, in which the carbene signal of $\mathbf{F_N1}$ from **IV** is observed to keep growing without being depleted [25]. This indicates that the complete mechanism, with inclusion of the catalytic cycle, should be investigated to make any concluding remarks. It has however been demonstrated by Halpern [33] that the most abundant complex in a solution need not be a part of the most favourable catalytic cycle;

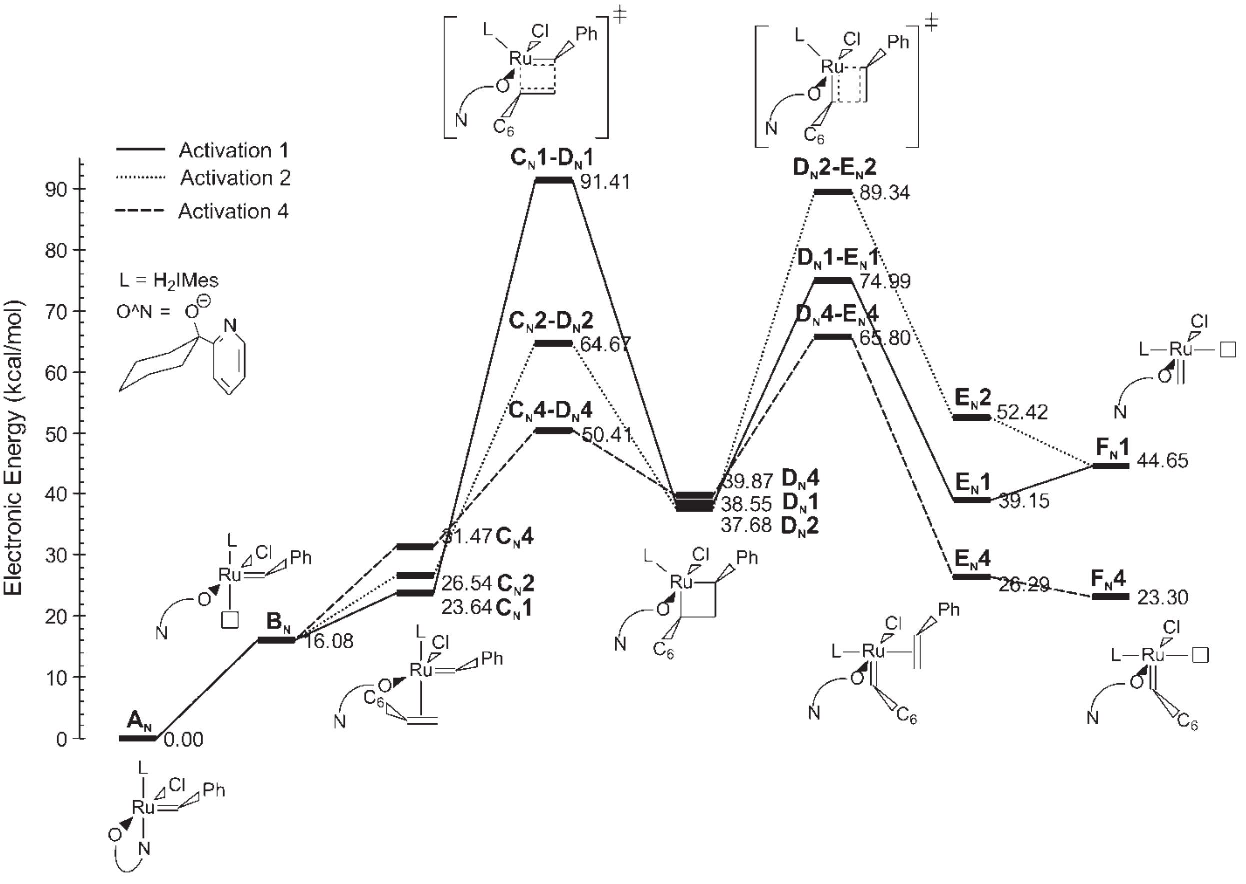

Figure 4. Electronic energy profiles of the activation steps in the productive 1-octene metathesis using **IV** (only the $\mathbf{C_N4}$ to $\mathbf{F_N4}$ structures are shown; $\mathbf{C_p}$ mode).

it may represent, in fact, a dead end. Therefore, the absence of $\mathbf{F_N1}$ in the ^{1}H NMR study of the 1-octene metathesis reaction with **III** [25] might suggest that a different mechanistic pathway is followed.

The calculated reaction energy for the formation of the ruthenacyclobutane intermediate (**III-**$\mathbf{D_N4}$) from the π-complex **III-**$\mathbf{C_N4}$ in the presence of **III** is endothermic (3.31 kcal/mol) for the $\mathbf{C_p}$ mode with activation energy of 31 kcal/mol (Figure 2). By contrast, the formation of '$\mathbf{D_N}$' from the π-complex '**C**' is exothermic for both activation steps 1 (−11.95 kcal/mol) and 2 (−4.51 kcal/mol) with activation energies of 66 and 45 kcal/mol, respectively. The decomposition of the ruthenacyclobutane ('$\mathbf{D_N}$' to '$\mathbf{E_N}$') is endothermic for both the heptylidene (15 kcal/mol) and methylidene (*ca.* 23 kcal/mol) formation steps with activation energies of *ca.* 45 and 70 kcal/mol, respectively. The coordination of the 1-octene in the $\mathbf{C_{II}}$ mode has a *ca.* 2–5 kcal/mol decrease in $\Delta E^{\ddagger}_{o}$ for '$\mathbf{D_N}$' to '$\mathbf{E_N}$' for all three activation steps, as well as for '$\mathbf{C_N}$' to '$\mathbf{D_N}$' in step 2 (Figure 3). Additionally, a 30 kcal/mol decrease in $\Delta E^{\ddagger}_{o}$ is observed for the formation of the ruthenacyclobutane in step 1, while step 4 shows a 2 kcal/mol increase. This indicates that the alkene prefers to coordinate with **III** in the $\mathbf{C_{II}}$ mode, in which the steric bulk around the Ru-centre is relieved in steps 1 and 2. This is due to the fact that the alkyl chain of 1-octene in steps 1 and 2 is no longer parallel to the Cl—Ru—O line, in which the alkyl chain was directly below the O,N-ligand and thereby adding to the steric bulk around the Ru-centre. The rate-limiting step for the formation of the heptylidene, as well as the methylidene species in the presence of **III**, is the decomposition of the ruthenacyclobutane ('$\mathbf{D_N}$' to '$\mathbf{E_N}$') for both coordination modes.

For **IV**, the decomposition of the ruthenacyclobutane ('$\mathbf{D_N}$' to '$\mathbf{E_N}$') in step 4 for both coordination modes (Figures 4 and 5), as well as the formation of '$\mathbf{D_N}$' from '$\mathbf{C_N}$' in step 1 for the $\mathbf{C_{II}}$ mode (Figure 5) is exothermic, i.e. approximately −13 and −1 kcal/mol, respectively. All the other formation or decomposition steps are endothermic for both the $\mathbf{C_p}$ and $\mathbf{C_{II}}$ modes. In contrast to **III**, different rate-limiting steps are involved in the formation of the heptylidene species from **IV** in the $\mathbf{C_p}$ and $\mathbf{C_{II}}$ modes, i.e. '$\mathbf{D_N}$' to '$\mathbf{E_N}$' for $\mathbf{C_p}$ (Figure 4) and '$\mathbf{C_N}$' to '$\mathbf{D_N}$' for $\mathbf{C_{II}}$ (Figure 5) with activation energy of 25.93 and 19.21 kcal/mol, respectively. The decomposition of the ruthenacyclobutane ('$\mathbf{D_N}$' to '$\mathbf{E_N}$')

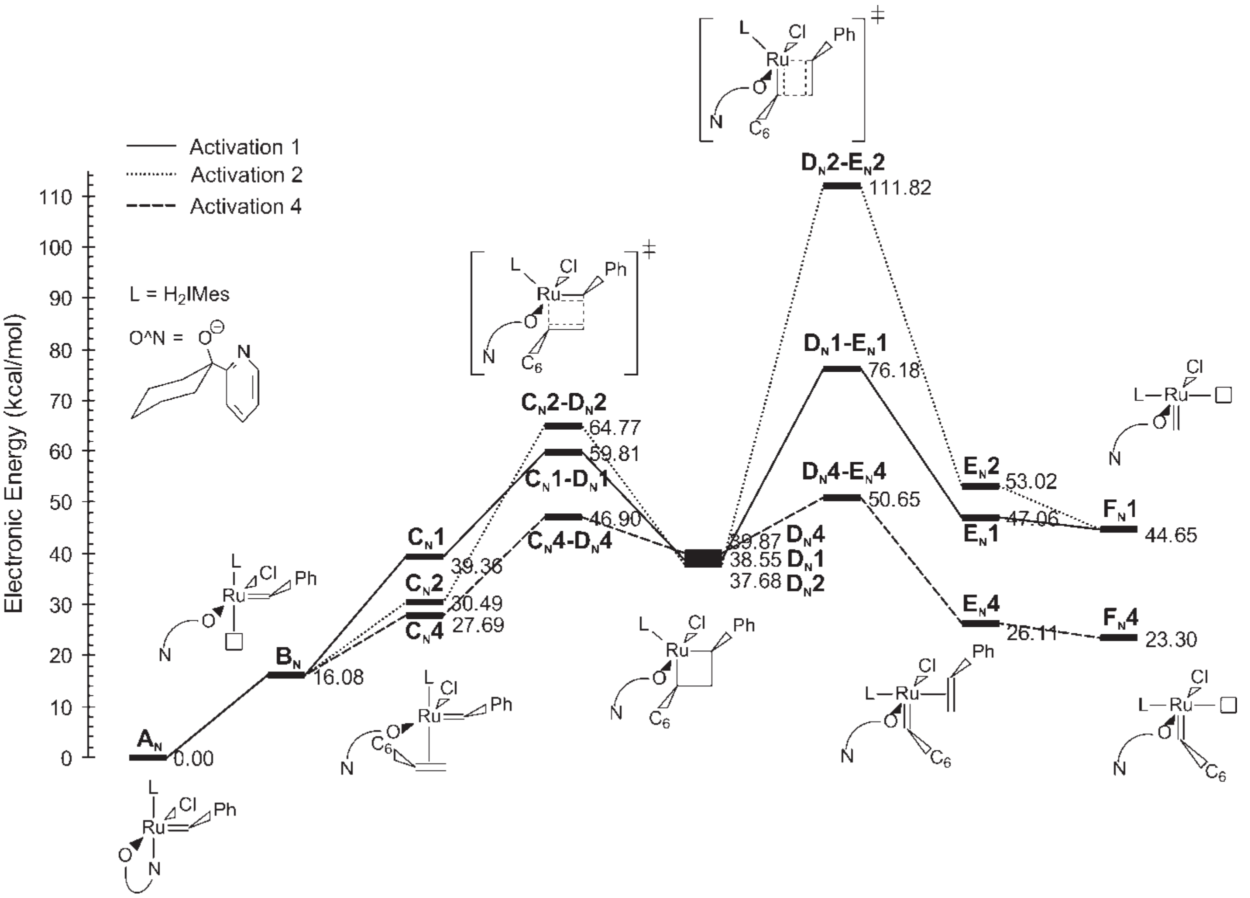

Figure 5. Electronic energy profiles of the activation steps in the productive 1-octene metathesis using **IV** (only the $\mathbf{C_N4}$ to $\mathbf{F_N4}$ structures are shown; $\mathbf{C_{II}}$ mode).

is considered the rate-limiting step for the formation of the methylidene species in steps 1 ($\Delta E^{\ddagger}_{\mathrm{o}\,\mathbf{D1-E1}} =$ 37.63 kcal/mol) and 2 ($\Delta E^{\ddagger}_{\mathrm{o}\,\mathbf{D2-E2}} = 74.14$ kcal/mol) in the $\mathbf{C_{II}}$ mode (Figure 5) as well as step 2 ($\Delta E^{\ddagger}_{\mathrm{o}\,\mathbf{D2-E2}} =$ 51.66 kcal/mol) in the $\mathbf{C_p}$ mode (Figure 4). The rate-limiting step for the formation of the methylidene species in step 1 in the $\mathbf{C_p}$ mode is the formation of the ruthenacyclobutane with an activation energy of 67.77 kcal/mol. No conclusions can be made regarding the preferred coordination mode of the alkene to **IV**, since mixed increasing and decreasing effects are observed with regards to the TS's. This might be due to the fact that the preliminary frequency analysis on the various TS's indicated that only $\mathbf{D_N1{-}E_N1}$ (263*i* cm^{-1}) and $\mathbf{C_N4{-}D_N4}$ (120*i* cm^{-1}) in the $\mathbf{C_p}$ mode (Figure 4) are close to a TS. The overall energy change from '$\mathbf{B_N}$' to '$\mathbf{F_N}$' for both the $\mathbf{C_p}$ and $\mathbf{C_{II}}$ mode for heptylidene formation in the presence of **III** and **IV** is 16.47 and 7.22 kcal/mol, respectively. For methylidene formation it is between 27 and 29 kcal/mol, respectively. The activation phase during the 1-octene metathesis reaction in the presence of **III** and **IV** is therefore strongly endothermic compared to **I** and **II** [8], which indicates that the hemilabile Ru–carbene complexes are relatively more stable compared to the Grubbs carbenes. Only after full frequency calculations have been performed to obtain the Gibbs free energies, will kinetic or thermodynamic stability of these complexes be confirmed.

Comparison of the activation steps of **III** and **IV** for the formation of the heptylidene species in the $\mathbf{C_{II}}$ mode (which is more favourable than the $\mathbf{C_p}$ mode; see Figure 6), suggests that **IV** is more active than **III**. Due to the endothermic nature of the sequence '$\mathbf{A_N}$' → '$\mathbf{B_N}$' → '$\mathbf{A_N}$' → '$\mathbf{B_N}$' → '$\mathbf{C_N}$' → '$\mathbf{C_N{-}D_N}$' (Figure 7) for both systems, the total barrier for ruthenacyclobutane ('$\mathbf{D_N}$') formation may be correlated to the energy change of '$\mathbf{A_N}$' → '$\mathbf{C_N{-}D_N}$' [12]. The largest barrier is calculated for **III** (62.03 kcal/mol), with **IV** (46.90 kcal/mol) exhibiting a much lower barrier. Therefore, relative reaction rates for these catalysts in decreasing order are suggested: **IV** > **III**, which is in qualitative agreement with the relative turnover numbers of these systems [25].

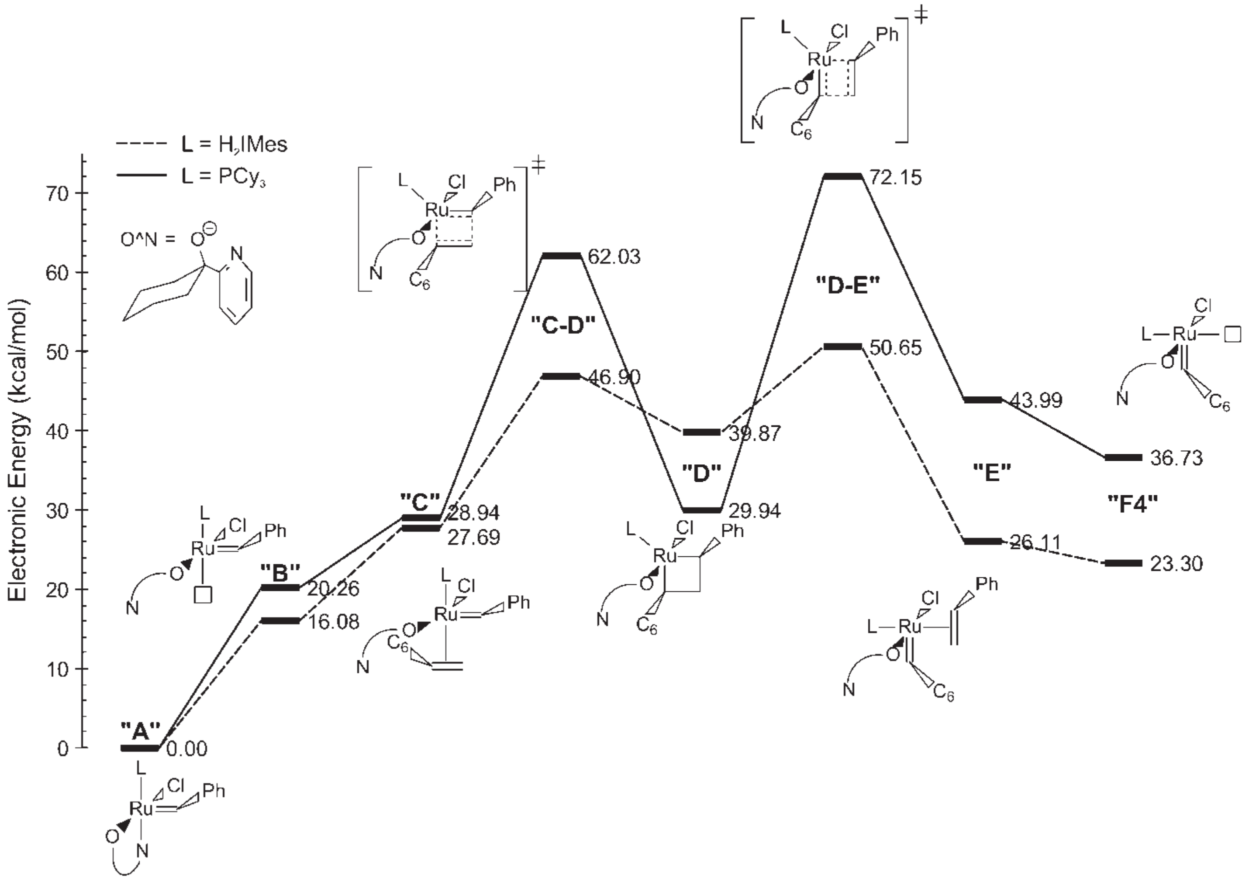

Figure 6. Comparison of the electronic energy profiles of the activation steps of **III** and **IV** in the productive 1-octene metathesis ($\mathbf{C_{II}}$ mode).

3.2.2 *Dissociation of ligand L from **III** and **IV***

The possibility of phosphine or NHC ligand dissociation from the respective first- and second-generation hemilabile carbenes should not be excluded, since it is generally assumed that ruthenium-catalysed metathesis reactions proceed through 14-electron intermediates [6,15,16,32]. Consequently, we have postulated a mechanism for the first- and second-generation hemilabile-catalysed 1-octene metathesis reaction (Scheme 2) whereby the O,N-ligand remains attached to the Ru-centre.

Experimental [15,32] and theoretical evidence [4–7,34] has shown that the phosphine, and not the NHC carbene, dissociates from **II** indicating that the intermediates for catalysis by first- and second-generation catalysts are different. Due to the higher binding energy of NHC ligands in comparison with phosphine ligands, the dissociation of the NHC ligand during the initiation step of the mechanistic cycle will result in higher dissociation energy [15,34]. This is most probably due to the increased σ-donor capability and the reduced π-acidity of the NHC ligand [35–37] in comparison with PR_3 ligands, which increase the stability of the second-generation catalysts. When applied to the hemilabile second-generation systems, it is clearly shown that the dissociation of the NHC ligand, which is 45 kcal/mol higher than the dissociation of the labile N-atom, will be improbable. Therefore, the activation phase resulting from initiation via dissociation of H_2IMes from **4** will not be considered further.

The activation steps for the $\mathbf{C_p}$ mode of **III** are graphically represented in Figure 7, while Figure 8 illustrates the steps for the $\mathbf{C_{II}}$ mode according to Scheme 2. The relative energies for the optimised structures are summarised in Table 3. Activation step 3 is not shown due to its similarity to activation step 4. No energy barriers were calculated for the dissociation of ligand L (L = PCy_3 or H_2IMes) or the association of the alkene, since it proceeds without considerable rearrangement of the complex.

Although the dissociation of PCy_3 from **III** is 3 kcal/mol higher compared with the dissociation of the labile N-atom of the O,N-ligand, more stable intermediates form during the activation phase for both the $\mathbf{C_p}$ and $\mathbf{C_{II}}$ modes (Figures 7 and 8). A decrease of approximately 15–30 kcal/mol is observed in the energies of the alkene-coordinated π-complexes, together with a 5–15 kcal/mol

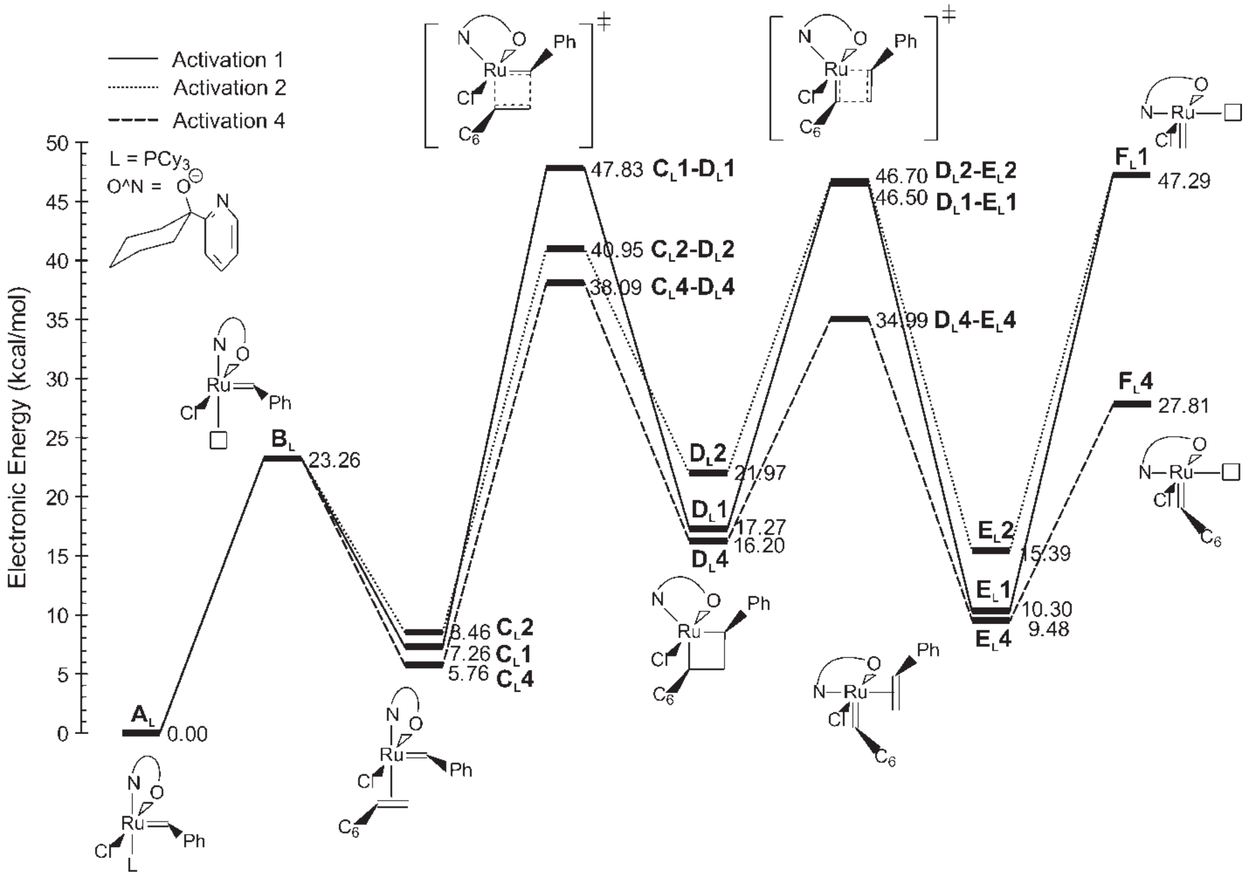

Figure 7. Electronic energy profiles of the activation steps in the productive 1-octene metathesis using **III** (only the $\mathbf{C_L4}$ to $\mathbf{F_L4}$ structures are shown; $\mathbf{C_p}$ mode).

decrease in the metallacyclobutane '**D**' species. A decrease was also noted in the TSs, which varied between 5 and 45 kcal/mol. Additionally, the overall energy changes from '$\mathbf{B_L}$' to '$\mathbf{F_L}$' for both the $\mathbf{C_p}$ and $\mathbf{C_{II}}$ modes decrease with 12 kcal/mol. This indicates that **III** most likely initiates according to Scheme 2 rather than Scheme 1, which explains why only three carbene species were observed during the ^{1}H NMR investigation [25].

Activation step 4 ($\mathbf{B_L}$ to $\mathbf{C_L4}$ to $\mathbf{F_L4}$) is thermodynamically and kinetically more favourable than activation steps 1 ($\mathbf{B_L}$ to $\mathbf{C_L1}$ to $\mathbf{F_L1}$) and 2 ($\mathbf{B_L}$ to $\mathbf{C_L2}$ to $\mathbf{F_L1}$; note $\mathbf{F_L2} = \mathbf{F_L1}$) for **III** in the $\mathbf{C_p}$ and $\mathbf{C_{II}}$ mode. The calculated reaction energy for the formation of the ruthenacyclobutane intermediate ('$\mathbf{D_L}$') from the π-complex '$\mathbf{C_L}$' in the presence of **III** is endothermic for the $\mathbf{C_p}$ (*ca.* 11 kcal/mol) and $\mathbf{C_{II}}$ (*ca.* 9 kcal/mol) mode for all the activation steps. By contrast, the formation of '$\mathbf{D_L}$' from the π-complex '$\mathbf{C_L}$' is exothermic for all the activation steps in the $\mathbf{C_p}$ (*ca.* -7 kcal/mol) and $\mathbf{C_{II}}$ (*ca.* -8 kcal/mol) mode. The coordination of the 1-octene in the $\mathbf{C_{II}}$ mode shows only a slight decrease in the activation energy of the ruthenacyclobutane formation and decomposition steps for activation steps 2 (1.92 kcal/mol decrease) and 4 (3.94 kcal/mol decrease), with a 1 kcal/mol increase for step 1. By contrast, a 12.59 kcal/mol increase was observed in $\Delta E_{\mathrm{o}}^{\ddagger}$ for '$\mathbf{D_L}$' to '$\mathbf{E_L}$' for step 1. This indicates that the alkene can coordinate with **III** in either mode. The rate-limiting step for the formation of the heptylidene ($\Delta E^{\ddagger} \approx 30$ kcal/mol) as well as the methylidene ($\Delta E_{\mathrm{o}}^{\ddagger} \approx 30$–$42$ kcal/mol) species in the presence of **III**, from which PCy_3 has dissociated, is the formation of the ruthenacyclobutane ('$\mathbf{C_L}$' to '$\mathbf{D_L}$') for both coordination modes.

4. Conclusions

The initiation and activation steps of **III** and **IV**, with 1-octene as substrate, were investigated to determine the catalytically active species that preferentially forms from the benzylidene precatalyst. Although it is generally accepted that the Grubbs carbenes initiate with the dissociation of PCy_3, this is not necessarily the case for the hemilabile complexes, since only one or no PCy_3 is present in the system. Therefore, these systems either initiate through the dissociation of the labile N-atom of the pyridine ring or through dissociation of L. Since

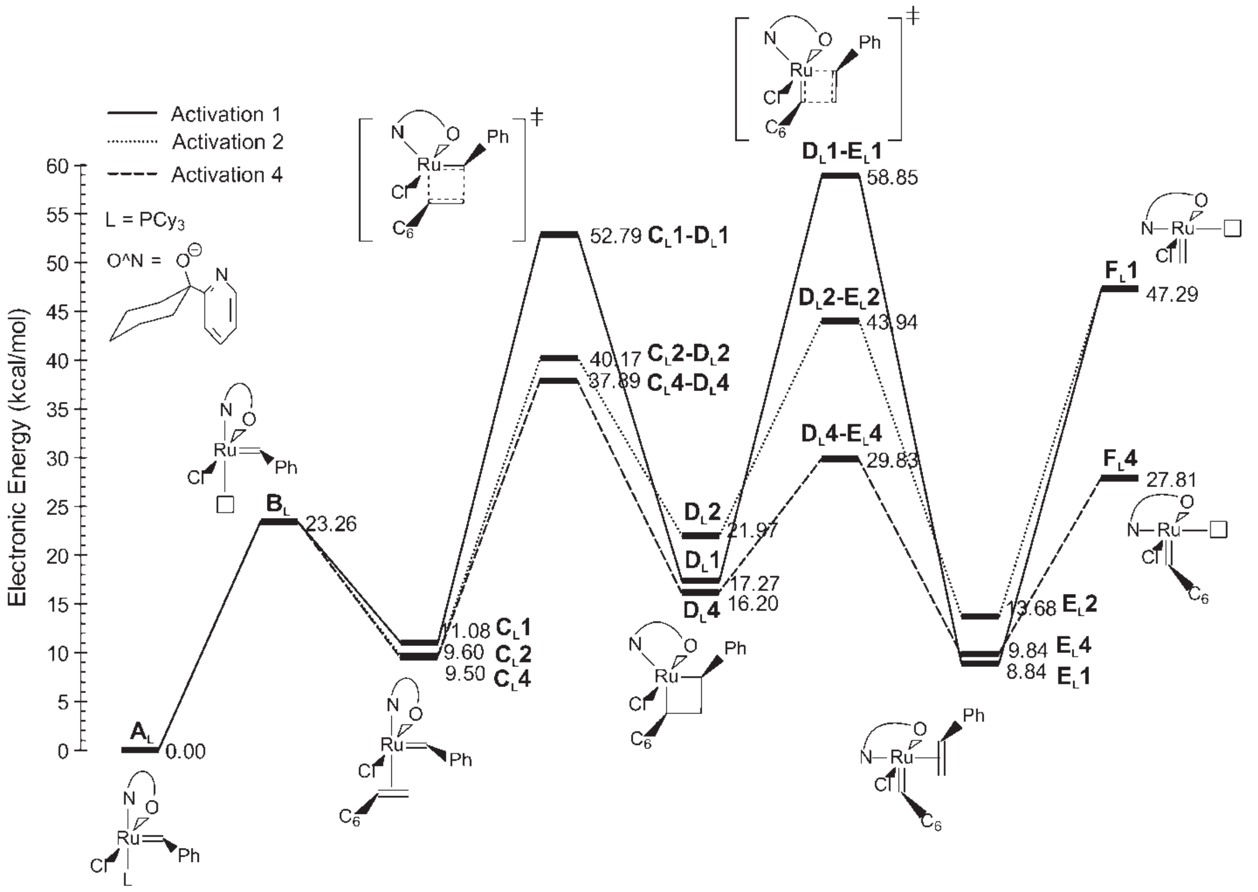

Figure 8. Electronic energy profiles of the activation steps in the productive 1-octene metathesis using **III** (only the $\mathbf{C_L4}$ to $\mathbf{F_L4}$ structures are shown; $\mathbf{C_{II}}$ mode).

Table 2. Calculated electronic (ΔE) energies and selected activation ($\Delta E^{\ddagger}_{o}$) energies in kcal/mol for the metathesis mechanistic sequence $\mathbf{A_N}$–$\mathbf{F_N}$ as catalysed by **III** and **IV**.

	III				**IV**			
Mechanistic sequence #	ΔE $\mathbf{C_p}$	$\Delta E^{\ddagger}_{o}$ $\mathbf{C_p}^{a}$	ΔE $\mathbf{C_{II}}$	$\Delta E^{\ddagger}_{o}$ $\mathbf{C_{II}}^{a}$	ΔE $\mathbf{C_p}$	$\Delta E^{\ddagger}_{o}$ $\mathbf{C_p}^{a}$	ΔE $\mathbf{C_{II}}$	$\Delta E^{\ddagger}_{o}$ $\mathbf{C_{II}}^{a}$
$\mathbf{A_N}$	0.00		0.00		0.00		0.00	
$\mathbf{B_N}$	20.26		20.26		16.08		16.08	
$\mathbf{C_N1}$	35.16		25.66		23.64		39.36	
$\mathbf{C_N2}$	31.06		23.14		26.54		30.49	
$\mathbf{C_N4}$	26.83		28.94		31.47		27.69	
$\mathbf{C_N1}$–$\mathbf{D_N1}$	101.21	66.05	59.29	33.63	91.41	67.77	59.81	20.45
$\mathbf{C_N2}$–$\mathbf{D_N2}$	71.60	40.54	65.95	42.81	64.67	38.13	64.77	34.28
$\mathbf{C_N4}$–$\mathbf{D_N4}$	46.76	19.93	62.03	33.09	50.41	18.94	46.90	19.21
$\mathbf{D_N1}$	23.41		23.41		38.55		38.55	
$\mathbf{D_N2}$	26.55		26.55		37.68		37.68	
$\mathbf{D_N4}$	30.14		29.94		39.87		39.87	
$\mathbf{D_N1}$–$\mathbf{E_N1}$	95.49	72.08	90.21	66.80	74.99	36.44	76.18	39.63
$\mathbf{D_N2}$–$\mathbf{E_N2}$	90.84	64.29	89.05	62.50	89.34	51.66	111.82	74.14
$\mathbf{D_N4}$–$\mathbf{E_N4}$	74.57	44.43	72.15	42.21	65.80	25.93	50.65	10.78
$\mathbf{E_N1}$	46.81		35.67		39.15		47.06	
$\mathbf{E_N2}$	49.54		42.81		52.42		53.02	
$\mathbf{E_N4}$	44.68		43.99		26.29		26.11	
$\mathbf{F_N1}$	47.09		47.09		44.65		44.65	
$\mathbf{F_N4}$	36.73		36.73		23.30		23.30	

All energies are reported relative to the respective precatalysts '**A**' and balanced with the energies of free ligand, where necessary.[a] $\Delta E^{\ddagger}_{o}$ calculated for the various TSs e.g. $\Delta E^{\ddagger}_{o}(\mathbf{C_N}1 - \mathbf{D_N}1) = \Delta E(\mathbf{D_N}1) - \Delta E(\mathbf{C_N}1)$.

Table 3. Calculated electronic (ΔE) energies in kcal/mol for the metathesis mechanistic sequence $\mathbf{A_L}$–$\mathbf{F_L}$ as catalysed by **III**.

	III			
	ΔE $\mathbf{C_P}$	$\Delta E^{\ddagger}_{o}$ $\mathbf{C_P}^{a}$	ΔE $\mathbf{C_{II}}$	$\Delta E^{\ddagger}_{o}$ $\mathbf{C_{II}}^{a}$
$\mathbf{A_L}$	0.00		0.00	
$\mathbf{B_L}$	23.26		23.26	
$\mathbf{C_L1}$	7.26		11.08	
$\mathbf{C_L2}$	8.46		9.60	
$\mathbf{C_L4}$	5.76		9.50	
$\mathbf{C_L1}$–$\mathbf{D_L1}$	47.83	40.57	52.79	41.71
$\mathbf{C_L2}$–$\mathbf{D_L2}$	40.95	32.49	40.17	30.57
$\mathbf{C_L4}$–$\mathbf{D_L4}$	38.09	32.33	37.89	28.39
$\mathbf{D_L1}$	17.27		17.27	
$\mathbf{D_L2}$	21.97		21.97	
$\mathbf{D_L4}$	16.20		16.20	
$\mathbf{D_L1}$–$\mathbf{E_L1}$	46.50	29.23	58.85	41.58
$\mathbf{D_L2}$–$\mathbf{E_L2}$	46.70	24.73	43.94	21.97
$\mathbf{D_L4}$–$\mathbf{E_L4}$	34.99	18.79	29.83	13.63
$\mathbf{E_L1}$	10.30		8.84	
$\mathbf{E_L2}$	15.39		13.68	
$\mathbf{E_L4}$	9.48		9.84	
$\mathbf{F_L1}$	47.29		47.29	
$\mathbf{F_L4}$	27.81		27.81	

All energies are reported relative to the respective precatalysts '**A**' and balanced with the energies of free ligand, where necessary.[a] $\Delta E^{\ddagger}_{o}$ calculated for the various TSs e.g. $\Delta E^{\ddagger}_{o}(\mathbf{C_L}1 - \mathbf{D_L}1) = \Delta E(\mathbf{D_L}1) - \Delta E(\mathbf{C_L}1)$.

hemilabile ligands are known to release a free coordination site 'on demand' of competing substrates such as an alkene and occupy it otherwise, the dissociation of the N-atom was considered as a viable route of initiation. The modelling results indicated that the dissociation of the labile N-atom of the pyridine ring for both hemilabile systems was more favourable than the dissociation of L. However, for **III** this dissociation is only 3 kcal/mol more favourable than the dissociation of L compared to 46 kcal/mol for **IV**. This indicates that the possibility of PCy_3 dissociation from **III** should not be excluded.

The modelling results of the activation steps for **III** and **IV** indicated that the formation of the methylidene was thermodynamically favoured, while the kinetically favoured species was predicted to be the heptylidene. The computational results are in agreement with the experimental results obtained with NMR for the 1-octene metathesis reaction with **IV**, in which the hemilability of the bidentate ligand is preferred above the dissociation of L [26]. However, further investigation into the metathesis mechanism with **III** is needed to determine whether a combination between phosphine ligand dissociation and hemilability of the bidentate ligand exist, since experimental and computational results are not in agreement. Although good correlations with experimental data were obtained in this study, more realistic correlations should be obtained with the completion of all the frequency analyses and if solvation effects are taken into account.

References

[1] H. Kawamura-Kuribayashi, N. Koga, and K. Morokuma, *An ab initio MO study on ethylene and propylene insertion into the titanium-methyl bond in CH_3TiCl^{2+} as a model of homogeneous olefin polymerization*, J. Am. Chem. Soc. 114 (1992), pp. 2359–2366.

[2] T. Ziegler, E. Folga, and A. Berces, *A density functional study on the activation of hydrogen–hydrogen and hydrogen–carbon bonds by Cp_2Sc—H and Cp_2Sc—CH_3*, J. Am. Chem. Soc. 115 (1993), pp. 636–646.

[3] G. Sini, S.A. Macgregor, O. Eisenstein, and J.H. Teuben, *Why is beta-Me elimination only observed in d0 early-transition-metal complexes? An organometallic hyperconjugation effect with consequences for the termination step in Ziegler–Natta catalysis*, Organometallics. 13 (1994), pp. 1049–1051.

[4] C. Adlhart and P. Chen, *Comparing intrinsic reactivities of the first- and second-generation ruthenium metathesis catalysts in the gas phase*, Helv. Chim. Acta. 86 (2003), pp. 941–949.

[5] C. Adlhart and P. Chen, *Ligand rotation distinguishes first- and second-generation ruthenium metathesis catalysts*, Angew. Chem., Int. Ed. 41 (2002), pp. 4484–4487.

[6] C. Adlhart and P. Chen, *Mechanism and activity of ruthenium olefin metathesis catalysts: The role of ligands and substrates from a theoretical perspective*, J. Am. Chem. Soc. 126 (2004), pp. 3496–3510.

[7] L. Cavallo, *Mechanism of ruthenium-catalyzed olefin metathesis reactions from a theoretical perspective*, J. Am. Chem. Soc. 124 (2002), pp. 8965–8973.

[8] M. Jordaan, P. van Helden, C.G.C.E. van Sittert, and H.C.M. Vosloo, *Experimental and DFT investigation of the 1-octene metathesis reaction mechanism with the Grubbs 1 precatalyst*, J. Mol. Catal. A: Chem. 254 (2006), pp. 145–154.

[9] S.F. Vyboishchikov, M. Bühl, and W. Thiel, *Mechanism of olefin metathesis with catalysis by ruthenium carbene complexes: Density functional studies on model systems*, Chem. Eur. J. 8 (2002), pp. 3962–3975.

[10] W. Janse van Rensburg, P.J. Steynberg, M.M. Kirk, W.H. Meyer, and G.S. Forman, *Mechanistic comparison of ruthenium olefin metathesis catalysts: DFT insight into relative reactivity and decomposition behavior*, J. Organomet. Chem. 691 (2006), pp. 5312–5325.

[11] W. Janse van Rensburg, P.J. Steynberg, W.H. Meyer, M.M. Kirk, and G.S. Forman, *DFT prediction and experimental observation of substrate-induced catalyst decomposition in ruthenium-catalyzed olefin metathesis*, J. Am. Chem. Soc. 126 (2004), pp. 14332–14333.

[12] S. Fomine, S.M. Vargas, and A. Tlenkopatchev, *Molecular modeling of ruthenium alkylidene mediated olefin metathesis reactions. DFT study of reaction pathways*, Organometallics 22 (2003), pp. 93–99.

[13] G.S. Forman, A.E. McConnell, R.P. Tooze, W. Janse van Rensburg, W.H. Meyer, M.M. Kirk, C.L. Dwyer, and D.W. Serfontein, *A convenient system for improving the efficiency of first-generation ruthenium olefin metathesis catalysts*, Organometallics 24 (2005), pp. 4528–4542.

[14] C. Adlhart, *Intrinsic reactivity of ruthenium carbenes: A combined gas phase and computational study*, (2003), Ph.D. thesis, Eidgenossische Technische Hochschule, Zurich.

[15] M.S. Sanford, J.A. Love, and R.H. Grubbs, *Mechanism and activity of ruthenium olefin metathesis catalysts*, J. Am. Chem. Soc. 123 (2001), pp. 6543–6554.

[16] C. Adlhart, C. Hinderling, H. Baumann, and P. Chen, *Mechanistic studies of olefin metathesis by ruthenium carbene complexes using electrospray ionization tandem mass spectrometry*, J. Am. Chem. Soc. 122 (2000), pp. 8204–8214.

[17] J. Louie and H. Grubbs, *Metathesis of electron-rich olefins: Structure and reactivity of electron-rich carbene complexes*, Organometallics 21 (2002), pp. 2153–2164.

[18] J. Huang, E.D. Stevens, S.P. Nolan, and J.L. Petersen, *Olefin metathesis-active ruthenium complexes bearing a nucleophilic carbene ligand*, J. Am. Chem. Soc. 121 (1999), pp. 2674–2678.

[19] K.A. Burdett, L.D. Harris, P. Margl, B.R. Maughon, T. Mokhtar-Zadeh, P.C. Saucier, and F.P. Wasserman, *Renewable monomer feedstocks via olefin metathesis: Fundamental mechanistic studies*

of methyl oleate ethenolysis with the first-generation Grubbs catalyst, Organometallics 23 (2004), pp. 2027–2047.

[20] F. Bernardi, A. Bottoni, and G.P. Miscione, *DFT study of the olefin metathesis catalyzed by ruthenium complexes*, Organometallics 22 (2003), pp. 940–947.

[21] K. Denk, J. Fridgen, and W.A. Herrmann, *N-Heterocyclic carbenes, part 33. Combining stable NHC and chelating pyridinyl-alcoholato ligands: A ruthenium catalyst for applications at elevated temperatures*, Adv. Synth. Catal. 344 (2002), pp. 666–670.

[22] C.W. Bielawski, *Tailoring polymer synthesis with designer ruthenium catalysts*, (2003), Ph.D. thesis, California Institute of Technology, California.

[23] C.S. Slone, D.A. Weinberger, and C.A. Mirkin, *The transition metal coordination chemistry of hemilabile ligands*, Progr. Inorg. Chem. 48 (1999), pp. 233–250.

[24] W.H. Meyer, R. Brull, H.G. Raubenheimer, C. Thompson, and J. Kruger, *Thioethercarboxylates in palladium chemistry: First proof of hemilabile properties of S—O ligands*, J. Organomet. Chem. 553 (1998), pp. 83–90.

[25] M. Jordaan and H.C.M. Vosloo, *Ruthenium catalyst with a chelating pyridinyl-alcoholato ligand for application in linear alkene metathesis*, Adv. Synth. Catal. 349 (2007), pp. 184–192.

[26] B. Delley, *An all-electron numerical method for solving the local density functional for polyatomic molecules*, J. Chem. Phys. 92 (1990), pp. 508–517, B. Delley, *From molecules to solids with the DMol3 approach*, J. Chem. Phys. 113 (2000) pp. 7756–7764; B. Delley, *Fast calculation of electrostatics in crystals and large molecules*, J. Phys. Chem. 100 (1996) pp. 6107–6110.

[27] J.P. Perdew and Y. Wang, *Accurate and simple analytic representation of the electron–gas correlation energy*, Phys. Rev. B 45 (1992), pp. 13244–13249.

[28] B. Delley, *DMol, a Standard Tool for Density Functional Calculations: Review and Advances,* in *Modern Density Functional Theory: A Tool for Chemistry, Theoretical And Computational Chemistry*, J. M. Seminario and P. Politzer, eds., Elsevier, Amsterdam, 1995, pp. 221–254.

[29] J. Andzelm, R.D. King-Smith, and G. Fitzgerald, *Geometry optimization of solids using delocalized internal coordinates*, Chem. Phys. Lett. 335 (2001), pp. 321–326.

[30] W. Janse van Rensburg, C. Grove, J.P. Steynberg, K.B. Stark, J.J. Huyser, and P.J. Steynberg, *A DFT study toward the mechanism of chromium-catalyzed ethylene trimerization*, Organometallics 23 (2004), pp. 1207–1222.

[31] G. Henkelman and H. Jonsson, *Improved tangent estimate in the nudged elastic band method for finding minimum energy paths and saddle points*, J. Chem. Phys. 113 (2000), pp. 9978–9985.

[32] M.S. Sanford, M. Ulman, and R.H. Grubbs, *New insights into the mechanism of ruthenium-catalyzed olefin metathesis reactions*, J. Am. Chem. Soc. 123 (2001), pp. 749–750.

[33] J. Halpern, *Mechanism and stereoselectivity of asymmetric hydrogenation*, Science. 217 (1982), pp. 401–407.

[34] T. Weskamp, F.J. Kohl, W. Hieringer, D. Gleich, and W.A. Herrmann, *Highly active ruthenium catalysts for olefin metathesis: The synergy of N-heterocyclic carbenes and coordinatively labile ligands*, Angew. Chem. Int. Ed. 38 (1999), pp. 2416–2419.

[35] J.P. Collman, L.S. Hegedus, J.R. Norton, and R.G. Finke, *Principles and Applications of Organotransition Metal Chemistry*, University Science Books, Mill Valley, CA, 1987.

[36] A.J. Arduengo III, *Looking for stable carbenes: The difficulty in starting anew*, Acc. Chem. Res. 32 (1999), pp. 913–921.

[37] L. Perrin, E. Clot, O. Eisenstein, J. Loch, and R.H. Crabtree, *Computed ligand electronic parameters from quantum chemistry and their relation to Tolman parameters, lever parameters, and Hammett constants*, Inorg. Chem. 40 (2001), pp. 5806–5811.